Magnetic properties of Fe films and Fe/Si/Fe trilayers grown on GaAs(001) and MgO(001) by ion-beam sputter epitaxy

Thorsten Damm,[a] Matthias Buchmeier, Alexandra Schindler, Daniel E. Bürgler,[b] Peter Grünberg, and Claus M. Schneider
Institut für Festkörperforschung, Forschungszentrum Jülich GmbH, D-52425 Jülich, Germany and Center of Nanoelectronic Systems for Information Technology (CNI), Forschungszentrum Jülich GmbH, D-52425 Jülich, Germany

(Received 5 April 2005; accepted 23 March 2006; published online 15 May 2006)

We grow monocrystalline Fe(001) films and Fe/Si/Fe(001) trilayers by ion-beam sputter epitaxy on GaAs(001) and MgO(001) substrates. Ion-beam sputtering parameters such as substrate presputtering time, substrate temperature, beam voltage, and target angle are optimized for 10-nm-thick Fe(001) films with respect to epitaxial growth and magnetic properties. *In situ* low-energy electron diffraction patterns confirm the epitaxial and monocrystalline nature of the sputtered films, surprisingly even on untreated and thus oxidized substrates. The magneto-optical Kerr effect and ferromagnetic resonance are employed to investigate the magnetic properties, and the structural properties are characterized by atomic force microscopy and x-ray reflectivity measurements. Using the optimized set of parameters that yields the best magnetic properties for single Fe films on GaAs, we deposit epitaxial Fe/Si/Fe(001) structures and observe antiferromagnetic interlayer exchange coupling for epitaxially sputtered Fe/Si/Fe(001) trilayers on GaAs(001). The total coupling strength reaches values of up to 2 mJ/m^2 at a Si thickness of 15 Å. © *2006 American Institute of Physics*. [DOI: 10.1063/1.2197034]

I. INTRODUCTION

Spintronics has recently become a very intensely discussed topic in the solid state physics community. The use of the spin degree of freedom of the electron in addition to its charge in spintronic devices promises additional functionalities,[1] increased data processing speed, less power consumption, and increased integration densities.[2] A key issue is the injection of spin polarized currents into semiconductors. The Fe/GaAs(001) system has been discussed as a candidate for spin injection right from the beginning[1] and was recently shown to exhibit a spin injection efficiency of 2% at room temperature in epitaxial samples grown by molecular beam epitaxy (MBE).[3]

Pioneering work on the epitaxial growth of Fe on GaAs(001) was performed by Krebs *et al.*[4] in 1987 by extending the MBE technique from semiconductors to metals. The epitaxial growth of this system is not restricted to MBE but can also be achieved by techniques employing sputtering,[5–11] which is the commonly used thin film deposition method in industry. The main interest of the studies mentioned above was on growth quality and magnetic properties with respect to substrate temperature and sputter geometry, but there are more parameters one can vary to influence the film growth. Especially the ion-beam sputtering technique is a powerful tool in this respect, since the sputtering parameters can be varied nearly independently over large ranges. The first part of this work deals with the growth optimization of 10-nm-thick, monocrystalline iron layers. In the second part we show results of epitaxially sputtered substrate/Fe/Si/Fe systems with strong antiferromagnetic interlayer exchange coupling as a further demonstration of the good film and interface quality.

II. EXPERIMENTAL PROCEDURES

The main focus of this work is to optimize the quality of an Fe layer which we deposit directly onto the substrate with respect to structural and magnetic properties. Therefore, the growth of 10-nm-thick Fe films on GaAs(001) and MgO(001) is first studied as a function of the following successively varied sputtering parameters: substrate presputtering time t, beam voltage U_{beam}, sputtering gas pressure p, substrate temperature T, and target angle φ (Table I). The optimized set of parameters leading to good epitaxy, smooth surfaces, and good magnetic properties is then used to grow Fe/Si/Fe trilayers with varying Si interlayer thickness.

The ion-beam sputtering system is ultrahigh vacuum (UHV) compatible and reaches a base pressure better than 10^{-9} mbar. A sample transfer allows to bring the samples to attached analysis chambers where low-energy electron diffraction (LEED) and x-ray photoemission spectroscopy (XPS) measurements can be performed *in situ*.

GaAs(001) and MgO(001) substrates of 10×10 mm^2 size are mounted without any preceding treatment at the same radius on a 4-in.-diameter sample holder. Rotation of the substrate holder at 5–8 rpm guarantees identical thicknesses of the films in one run. The sputtering rate is kept constant at 0.3 Å/s. The sputtering system is equipped with a 2 in. rf ion gun, which is aligned towards the target (sputter gun) and a 4 in. electron cyclotron resonance (ECR) gun,

[a]Present address: Sensitec naomi GmbH, Mainz, Germany. Electronic mail: thorsten.damm@naomi-mainz.de
[b]Electronic mail: d.buergler@fz-juelich.de

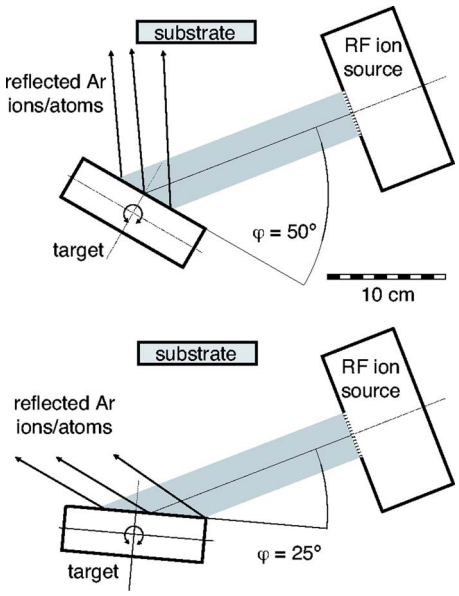

FIG. 1. Sputtering geometry for the two target angles $\varphi=25°$ and 50°. The assist gun is not shown for clarity.

FIG. 2. LEED pattern of a GaAs(001) surface taken at an electron energy of 108 eV after 15 s presputtering at $T=225$ °C, $U_{beam}=0.30$ kV, and $I_{beam}=30$ mA. The spots are remarkably sharp, and the pattern does not indicate any surface reconstruction.

which is aligned towards the substrate (assist gun). The sputtering geometry is shown in Fig. 1. The targets can be rotated (target angle φ) about the axis perpendicular to the incident ion beam and parallel to the plane of the substrate in order to vary the orientation of the sputter plume and the influence of reflected ions (or atoms after neutralization) on the growing film.[7] The average target-to-substrate distance (measured from target center to substrate center) is 13 cm and therefore of the same order of magnitude as the mean free path for our typical sputtering gas pressure of 10^{-3}-10^{-4} mbar. We use an Fe and a Si target with a purity of 99.95% and 99.999%, respectively. In order to prevent a charging of the Si target due to the bombardment with positive Ar ions, a beam-switch electronics is used. It allows to pulse the ion beam with frequencies between 1 and 20 kHz with varying duty cycles. During the periods of no ion acceleration the sputter gun's grid voltages can be inverted, so that electrons are extracted from the plasma. This broad electron beam hits the target and neutralizes any positive surface charge. Furthermore, this beam-switch electronics can also be used to influence the deposition rate without changing any other sputtering parameter. The film thicknesses are monitored by a quartz crystal microbalance.

Atomic force microscopy images are taken *ex situ* in tapping mode using a multimode scanning probe microscope (SPM) from Digital Instruments. We employ a Bruker-AXS diffractometer with Cu Kα radiation for low-angle x-ray reflectivity (XRR) measurements. Magneto-optical Kerr effect (MOKE) experiments are performed in the longitudinal geometry with the field applied along Fe(001)⟨100⟩. Ferromagnetic resonance (FMR) is observed by inserting a 2×2 mm^2 sample piece in a cylindrical resonator with adjustable length. The cylinder axis is in the sample plane. A stepper motor allows to rotate the sample about its surface normal. The static external field is applied perpendicular to both the rotation axis and the cylinder axis. In this way we can perform angle-dependent FMR measurements to determine magnetic in-plane anisotropies. The high frequency excitation (typically 8 GHz) is generated by a network analyzer and coupled to the resonator via an antenna, which simultaneously acts as a receiver to measure the reflection coefficient.

TABLE I. Variation of the sputtering parameters: substrate presputtering time t, substrate temperature T, beam voltage U_{beam}, and sputtering gas pressure p.

t (s)	T (°C)	U_{beam} (kV)	p (mbar)
0–200	225	0.75	10^{-3}
15	25–300	0.75	10^{-3}
15	225	0.30–1.30	10^{-4}

III. RESULTS AND DISCUSSION

A. Substrate preparation

The oxide and contamination layer on the GaAs and MgO substrates are removed by presputtering the substrates at the standard substrate temperature of $T=225$ °C with the Ar ion beam of the assist gun. The beam energy is $U_{beam}=0.30$ kV, and the beam current $I_{beam}=30$ mA corresponds to a current density at the position of the substrate of the order of 0.3 mA/cm^2. The amount of remaining oxygen on GaAs after different presputtering times t is calculated from XPS spectra by comparing the O-1s and Ga-3d peaks after different presputtering times t [Fig. 4(b)]. The oxygen signal decreases by a factor of 40 and drops below the detection limit of less than 1% after 15 s preputtering.

Untreated samples do not show a LEED pattern demonstrating that the oxide and contamination layers formed due to air exposure are disordered. However, after 5 s of presputtering, LEED spots appear and show the expected pattern for a cubic system (an example for 15 s presputtering is shown in Fig. 2). It is noteworthy that in contrast to removing the oxygen by heating (as usually done for MBE growth, e.g., Refs. 12 and 13), sputtering GaAs at $T=225$ °C leads to a

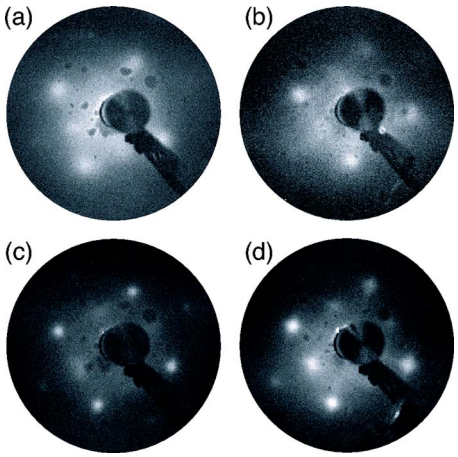

FIG. 3. LEED patterns of 10 nm Fe on (a) untreated GaAs, (b) presputtered GaAs(001), (c) untreated MgO, and (d) presputtered MgO(001). The presputtering time for (b) and (d) is $t=15$ s. Patterns are taken at 107 and 110 eV for Fe on GaAs and Fe on MgO, respectively.

nonreconstructed surface. For presputtering times of 40 s and longer, no LEED spots can be found indicating that the prolonged bombardment of the wafer with Ar ions destroys the crystallinity at the surface.

B. Single Fe films

Starting from a predefined standard set of sputtering parameters, 10 nm Fe is deposited on GaAs(001) and MgO(001) substrates and then the sputtering conditions are systematically varied as summarized in Table I. The standard parameters are $U_{\text{beam}}=0.75$ kV, $T=225$ °C, $p=1.8\times10^{-3}$ mbar, $t=15$ s, and $\varphi=50°$. The sputtering rate for all iron films is kept constant at 0.3 Å/s.

1. Variation of presputtering time

LEED data of the Fe films clearly prove that monocrystalline and epitaxial growth is achieved for *all* of the chosen presputtering times, even when the substrate does not show a LEED pattern, e.g., for no ($t=0$ s) or very long ($t=200$ s) presputtering. Figure 3 shows LEED patterns of 10-nm-thick Fe films grown on both substrate types in the untreated ($t=0$ s) and presputtered ($t=15$ s) state. We observe in all cases a square lattice with lattice constants corresponding to a (001) surface of bcc Fe. The Fe films grown on MgO(001) show slightly superior quality. The appearance of clear reciprocal lattices proves the monocrystallinity of the Fe films, whereas the orientation of the lattice with respect to the substrate crystal axes (determined from LEED patterns or the edges of the substrates) reveals the following epitaxial relationships: Fe(001)⟨100⟩‖GaAs(001)⟨100⟩ and Fe(001)⟨100⟩‖MgO(001)⟨110⟩. Figure 4(a) depicts the dependence of the coercive field H_c on the substrate presputtering time t for 10-nm-thick Fe for both substrate types. Fe films on MgO are magnetically softer than on GaAs indicating a better growth quality on MgO. The coercivity increases monotonously with t, and the lowest coercivity for both substrates is found for $t=0$. This means that—surprisingly—the growth on untreated, oxidized substrates is better than on presputtered ones. The evolution of the root-mean-square

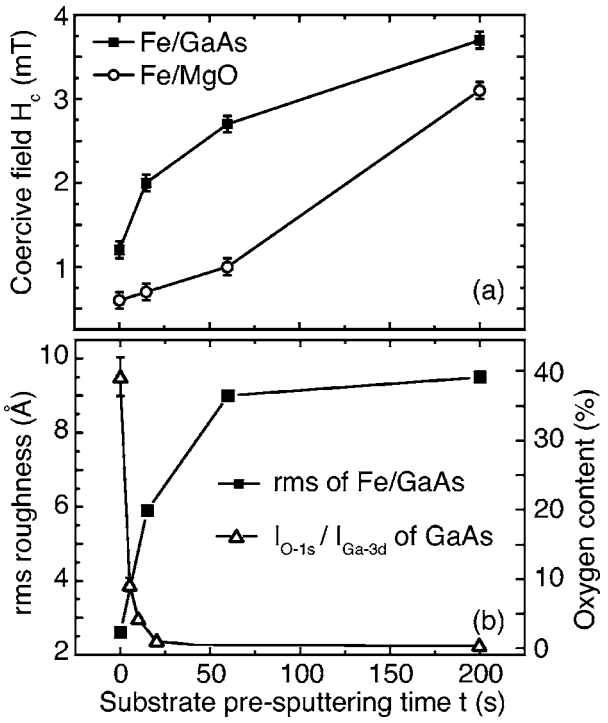

FIG. 4. (a) Coercive fields derived from MOKE measurements and (b) rms roughness derived from 1 μm^2 AFM pictures of 10-nm-thick Fe films on GaAs (squares) and MgO (circles) substrates as a function of the presputtering time t. Triangles in (b) show the evolution of oxygen content (I_{O-1s}/I_{Ga-3d}) of GaAs(001) substrates with presputtering time t.

(rms) roughness derived from atomic force microscopy (AFM) measurements with the presputtering time t [Fig. 4(b)] indicates that the cleaning process by ion bombardment roughens the substrate surface. The increased roughness gives rise to a higher density of pinning centers and, thus, the increased coercivity.

Angle-dependent FMR measurements shown in Fig. 5 confirm the MOKE results. For the presputtered GaAs substrate we find in Fig. 5(a) the fourfold magnetocrystalline anisotropy and a superimposed twofold anisotropy with the easy axis at 135°. This uniaxial anisotropy is well known[4,14] and appears whenever Fe is grown on clean GaAs(001) surfaces irrespective of its reconstruction prior to the deposition.[15] It arises from the (chemical) twofold symmetry of the GaAs(001) surface and is thus a pure interface anisotropy.[16] As the Fe thickness is kept constant in this study, interface and volume anisotropy contributions cannot be separated, and we always state *effective* anisotropy constants for the given Fe thickness of 10 nm. The anisotropy constants and the effective saturation magnetization M_S^{eff} are derived from fitting the FMR data using the standard procedure.[17,18] We find a twofold anisotropy for all GaAs samples for which the oxide layer is removed by a presputtering treatment [e.g., Fig. 5(a)]. All the more it is surprising that for untreated GaAs substrates as in Fig. 5(b), the uniaxial anisotropy is missing while the fourfold magnetocrystalline anisotropy is still there. Solid lines in Fig. 5 are the fits, and the fitting results are summarized in Table II.

A corresponding angle-dependent FMR measurement of a 10-nm-thick Fe film on untreated MgO is displayed in Fig.

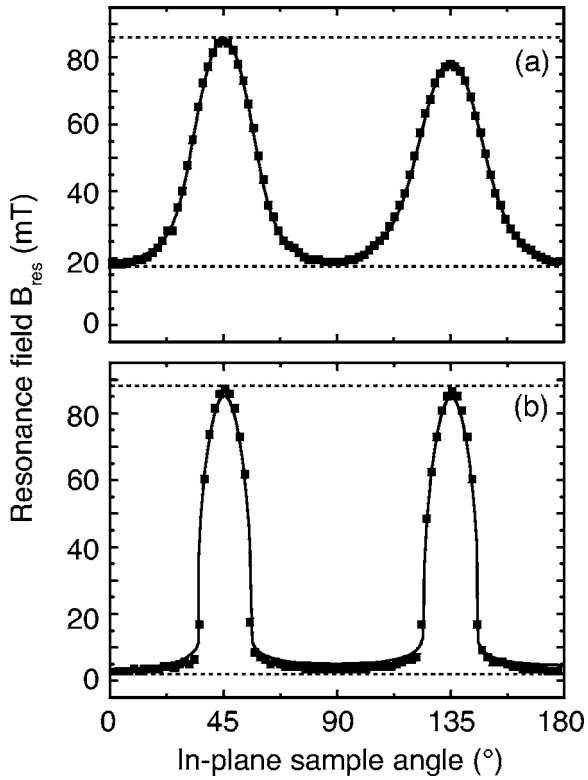

FIG. 5. Angle-dependent FMR measurement of 10-nm-thick Fe films on (a) presputtered GaAs and (b) untreated GaAs. The excitation frequency is 8 GHz. Squares represent data and the solid lines are best fits. At an in-plane sample angle of 0° the external field is parallel to an in-plane easy axis [i.e., Fe(001)⟨100⟩], and at 45° it is parallel to an in-plane hard axis of bcc Fe [i.e., Fe(001)⟨110⟩].

6(a) and reveals so called "loops." They are the result of the large magnetocrystalline anisotropy as compared to the low excitation frequency of 8 GHz. The resonance condition is fulfilled only in a small angle range ($\approx \pm 5°$) around the hard axes at 45° and 135°. This behavior is well reproduced by our fits [circles, Fig. 6(a)] and is explained in Fig. 6(b), where we plot the calculated resonance frequency as a function of the applied field for different in-plane sample angles θ using the film parameters derived from the fit in Fig. 6(a). Parameters for other deposition conditions on MgO are listed in Table II. The resonance condition is fulfilled when in Fig. 6(b) the horizontal line at the chosen excitation frequency of 8 GHz intersects with the calculated lines. This happens only for $\theta > 40°$ but then for each angle at *two* different magnetic fields. The distance of the two resonance fields varies strongly with θ: It is largest when the external field is parallel to the hard axis (i.e., at $\theta = 45°$) and becomes zero (meaning that only *one* resonance field exists) somewhere between $\theta \approx 40°$ and 41°. Thus, when plotting the resonance field(s) as a function of the in-plane sample angle θ, loops as in Fig. 6(a) appear.

TABLE II. Effective saturation magnetization M_S^{eff}, effective fourfold magnetocrystalline and uniaxial anisotropy constants, K_1^{eff} and K_u^{eff}, and their ratio $K_u^{\text{eff}}/K_1^{\text{eff}}$ derived from angle-dependent FMR data for 10-nm-thick Fe films grown on GaAs and MgO under conditions deviating from the standard parameters as indicated. The last line gives bulk values (Ref. 19) for comparison.

Deposition condition	M_S^{eff} (10^6 A/m)	K_1^{eff} (10^3 J/m^3)	K_u^{eff} (J/m^3)	$K_u^{\text{eff}}/K_1^{\text{eff}}$ (%)
		Fe on GaAs		
Standard	1.10	17.8	1900	11
$t=0$ s	1.26	25.6	190	1
$t=200$ s	0.90	15.4	4200	27
$\varphi=25°$	0.94	12.8	320	3
$U_{\text{beam}}=1.3$ keV	1.19	27.0	1200	4
$T_S=40$ °C	1.59	38.0	3800	10
		Fe on MgO		
Standard	1.50	43.3	1770	4
$t=0$ s	1.48	41.9	2600	6
$t=200$ s	1.47	36.1	<100	<1
$T_S=40$ °C	1.48	39.5	1300	3
Bulk bcc Fe	1.71	48.0		

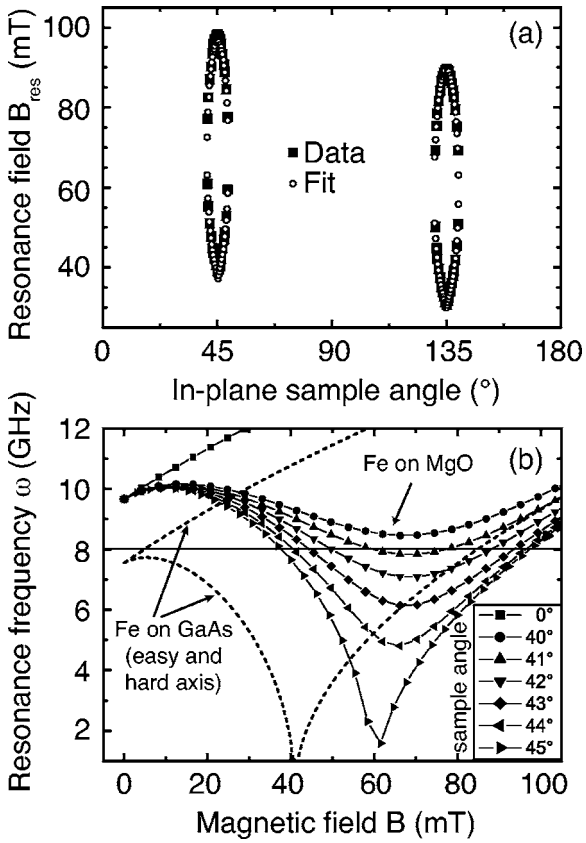

FIG. 6. (a) Angle-dependent FMR measurement of 10-nm-thick Fe films on untreated MgO. The excitation frequency of 8 GHz and the geometry is the same as in Fig. 5. Squares represent data and the circles are best fits. (b) Calculated resonance frequencies for different in-plane sample angles θ for untreated MgO (symbols) and untreated GaAs (dashed) for the explanation of the loops appearing in (a) but not in the curves of Fig. 5.

The dashed lines in Fig. 6(b) represent calculations for Fe on untreated GaAs, using the fitted film parameters from Fig. 5(b). Due to the lower magnetocrystalline anisotropy, for each sample angle θ only one resonance field exists, leading to the curve shape with peaks in Fig. 5(b).

An inspection of M_S^{eff} and K_1^{eff} values in Table II verifies that the quality of Fe on MgO substrates is better than the quality of Fe films on GaAs, as was derived from superior LEED patterns before.

A closer look at the parameters for Fe films on GaAs reveals that Fe films grown on untreated GaAs substrates (entry $t=0$ s in Table II) show a higher saturation magnetization as well as a larger magnetocrystalline anisotropy constant compared to the films grown under standard conditions (i.e., with $t=15$ s presputtering). In agreement with the results of the MOKE hysteresis loops, the Fe films on untreated GaAs substrates seem to have better crystallinity. Obviously, the cleaning process with Ar ions does not only remove the oxide at the surface but also damages the substrate's crystal structure. The effective uniaxial anisotropy constant is found to increase by one order of magnitude when the GaAs substrates are presputtered and reaches values of up to 27% of the fourfold magnetocrystalline anisotropy constant. Thus, the Fe films on untreated GaAs substrates grow—in accordance with the LEED data—as a monocrystalline layer. But they do not significantly experience the twofold symmetry of the bare GaAs(001) surface because the special Fe/GaAs bonding at the interface cannot form with the oxide layer being between them. We also find a weak twofold magnetic anisotropy for Fe films on MgO. The uniaxial anisotropy constant K_u^{eff} never exceeds a few percent of K_1^{eff} and—in contrast to the GaAs case—decreases with longer presputtering time t (Table II). Most likely, this uniaxial anisotropy is related a small miscut of the MgO(001) substrates as reported previously.[20–22]

Although our data clearly evidence monocrystalline growth of Fe on untreated, oxidized, and contaminated GaAs(001) and MgO(001) substrates, it is up to now not clear in detail what gives rise to the monocrystalline growth in spite of the disordered, oxidized substrates. The previous report[23] of epitaxial growth of Cr and Fe/Cr bilayers with Cr as a buffer and adhesion layer on untreated GaAs(001) did not address this question. One possible explanation could be that holes in the oxide layer exist. Since sputtered particles have an energy of several eV (sputtered atoms have a broad energy distribution with an average energy of the order of 10 eV), they also have a high mobility at the substrate surface, such that they can reach these holes and form growth seeds where crystalline growth nucleates. Several attempts to achieve epitaxial growth on identical, oxidized GaAs wafers by MBE, where atoms arrive at the surface with an energy of the order of 0.1 eV, failed. Thus, it seems that the high particle energy due to the sputtering process is indispensable. High-energetic Fe atoms with energies close to the sputtering threshold (10–30 eV) may help to form the crystalline nuclei.

2. Influence of target angle and beam voltage

Due to the given geometry of sputter gun, target, and substrate in our deposition chamber, it is likely that Ar ions specularly reflected from the target hit the substrate.[24,25] In order to check the presence of such reflected Ar ions and their influence on the (monocrystalline) growth, we vary the target angle such that possibly reflected Ar ions will not hit the substrate (Fig. 1). Comparing the angle-dependent FMR results of this sample (entry $\varphi=25°$ in Table II) with a sample prepared under standard conditions (i.e., $\varphi=50°$), we find lower values for the magnetocrystalline anisotropy constant ($K_1^{\text{eff}}=12.8$ kJ/m^3) and the saturation magnetization ($M_S^{\text{eff}}=0.94$ MA/m). This clearly demonstrates that reflected Ar ions do exist, and—in contrast to other work[11,26]—these high-energetic particles support the growth in a positive way. In the standard geometry, the situation is similar to ion-beam assisted deposition,[27] where ions of the assist gun bombard the sample while depositing the layer. Being aware of the reflected Ar ions, one expects an influence of the ion energy given by the beam voltage U_{beam} on the growth. Using the simple model from Bernstein *et al.*,[7] one estimates the reflected particle energy for our geometry to be 10% of the primary ion energy. Figure 7 shows the correlation between U_{beam} and coercivity, magnetocrystalline anisotropy, and effective saturation magnetization, respectively. In order to prevent arcs between the grids of the sputter gun at high voltages, we employ a lower Ar gas pressure of 3×10^{-4} mbar for these measurements. Increasing U_{beam} leads to a better crystallinity as can be seen in the increase of K_1^{eff} and M_S^{eff} (see also entry $U_{\text{beam}}=1.3$ keV in Table II). A low coercivity is obtained at an intermediate beam voltage of $U_{\text{beam}}\approx800$ V. Very low ion energies do not improve the growth, while high ion energies lead to defects in the film. They act as pinning centers for the magnetization and, therefore, increase the coercivity. In order to check whether the monocrystalline growth on untreated substrates is related to a sputtering effect of the reflected Ar ions, which possibly could remove the oxide, we deposit Fe on GaAs at different target angles φ with and without substrate presputtering. LEED spots (Fig. 8) confirm the monocrystalline growth of Fe on presputtered, clean as well as untreated GaAs at a target angle of $\varphi=25°$, where no ions from the target are

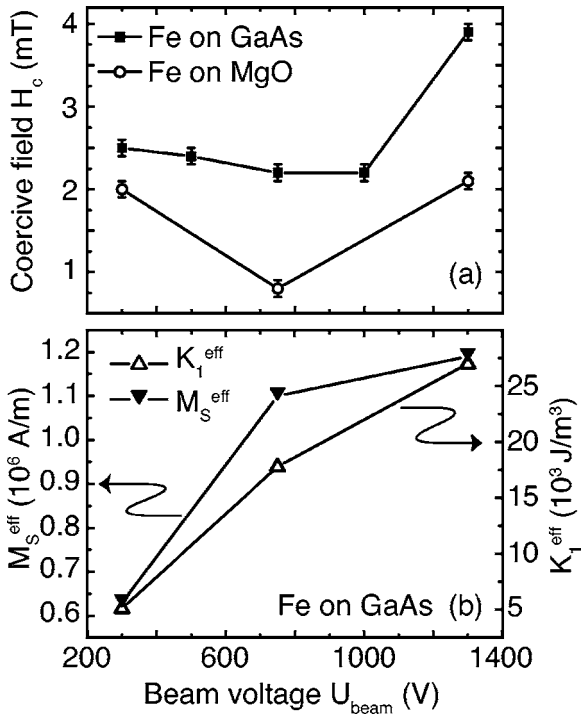

FIG. 7. Coercivity H_C, K_1^{eff}, and M_S^{eff} vs U_{beam}. The data in (b) are from Fe films on GaAs. Varying U_{beam} in the shown range is only possible at a lower pressure range (3×10^{-4} mbar). A higher pressure leads to arcs between the two grids of the sputter gun for $U_{\text{beam}}>1$ kV.

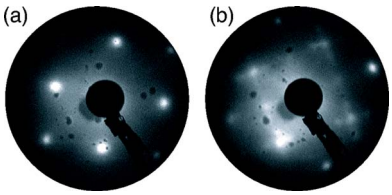

FIG. 8. LEED patterns of 10 nm Fe on (a) untreated, oxidized and (b) presputtered GaAs(001) at a target angle $\varphi=25°$, which prevents a reflection of Ar ions towards the substrate.

reflected towards the substrate. Thus, there is no sputtering of the oxide by reflected Ar ions. An interesting point is that—judging from the LEED spots—the growth on untreated substrates [Fig. 8(a)] is better than in case of substrate cleaning by presputtering [Fig. 8(b)]: Without treatment one finds nice, round spots while presputtering leads to additional spots and intensity around the main spots.

3. Substrate temperature

The substrate temperature turns out to be a very important parameter. While for Fe on MgO epitaxial growth takes place for all temperatures up to 300 °C, polycrystalline growth is found for Fe on GaAs at temperatures higher than 225 °C. XPS spectra of these samples (not shown here) reveal clear peaks for Ga and As, indicating strong interdiffusion of the substrate material and the Fe film. The best results for the growth of Fe on GaAs are achieved at 40 °C, as can be seen from Fig. 9, yielding $K_1^{\text{eff}}=38\ \text{kJ/m}^3$ and $M_S^{\text{eff}}=1.59$ MA/m (entry $T_S=40$ °C in Table II) very close to the Fe bulk values (last line in Table II). The high growth quality of the Fe film is supported by AFM measurements that reveal one of the lowest rms roughnesses ($\sigma_{\text{rms}}=2.8$ Å) of this study for deposition at 40 °C. The uniaxial effective anisotropy constant $K_u^{\text{eff}}=3800\ \text{J/m}^3$ amounts to about 30% of the value expected based on the result of Moosbühler *et al.*[15] for MBE-grown Fe films on GaAs(001) ($K_u^{\text{Fe/GaAs}}=0.13\ \text{mJ/m}^2$ and our Fe thickness of 10 nm). The lower value arises from the higher disorder and roughness of our substrates after the presputtering process compared to the carefully annealed substrates of Ref. 15.

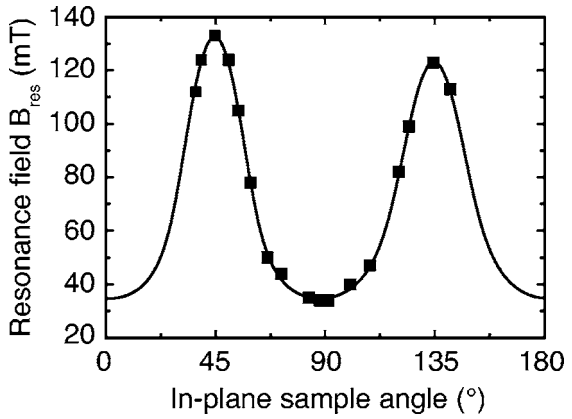

FIG. 9. FMR measurement of 10 nm Fe on GaAs deposited at 40 °C. Squares are the data and the line represents the best fit yielding the magnetic parameters listed as entry $T_S=40$ °C in Table II.

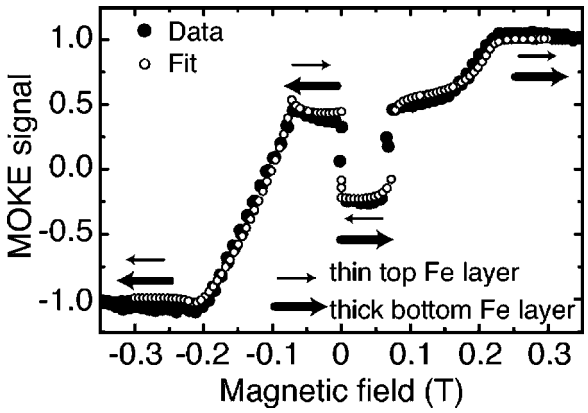

FIG. 10. MOKE loop of a 100 Å Fe/14 Å Si/50 Å Fe trilayer on GaAs. Filled circles represent data and open circles the best fit. The coupling parameters are $J_1=-0.81\ \text{mJ/m}^2$ and $J_2=-0.15\ \text{mJ/m}^2$. The arrows indicate the magnetization directions of the thin, top and thick, bottom Fe layer, respectively.

Very good epitaxial growth at this rather low temperature has not been found in previous work[6,7] and can be attributed to the reflected Argon ions. As in the case of ion-beam assisted deposition, the additional energy helps to increase the surface diffusion of the deposited particles, mimicking a higher substrate temperature. At other target angles, which prevent the substrate bombardment by reflected argon ions, inferior epitaxial film growth takes place as derived from FMR measurements.

C. Fe/Si/Fe trilayers

Using the sputtering parameters that lead to the best growth of Fe on GaAs (deposition at 40 °C, 15 s presputtering, $\varphi=50°$, $U_{\text{beam}}=0.75$ kV, and 1.8×10^{-3} mbar Ar pressure), a series of substrate/100 Å Fe/x Å Si/50 Å Fe trilayers with varying Si thickness x is deposited, where substrate stands for GaAs(001) and MgO(001). LEED patterns confirm the monocrystalline and epitaxial growth of the whole trilayer stack. MOKE measurements clearly show the presence of antiferromagnetic interlayer coupling for the trilayers on both substrate types. An example with a GaAs(001) substrate and a Si spacer thickness $x=14$ Å is shown in Fig. 10. The peculiar shape of the loop with the jump in small fields can be understood by taking into account that the *thinner* top Fe layer contributes *stronger* to the MOKE signal than the thicker bottom Fe layer. The reasons are the limited penetration depth of the laser light and reflections at the Fe/Si interfaces. Additionally, the signal contains strong second order MOKE effects due to a large angle of incidence (only about 15° from the sample normal), which give rise to further asymmetries with respect to zero field. Taking all these effects into account, we are able to well reproduce the MOKE loops (see arrows and circles in Fig. 10) and fit the bilinear and biquadratic coupling constants J_1 and J_2 defined by the phenomenological expression for the areal free energy density of the coupling,

$$E=-J_1\cos(\Delta\vartheta)-J_2\cos^2(\Delta\vartheta), \tag{1}$$

where $\Delta\vartheta$ is the angle between the magnetizations of the two ferromagnetic layers. We take into account the in-plane four-

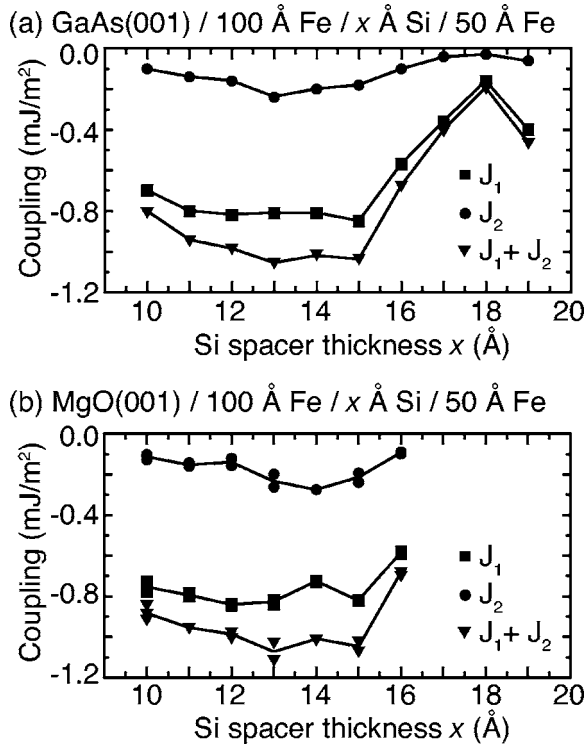

FIG. 11. Spacer thickness dependence of the coupling parameters J_1, J_2, and total coupling strength $J=J_1+J_2$ derived by fitting MOKE loops of Fe/Si/Fe trilayers on (a) GaAs and (b) MgO substrates.

fold magnetocrystalline anisotropy, the Zeeman energy, and the possible twisted magnetization state within each ferromagnetic layer.[28]

The variation of the coupling strengths as a function of the Si spacer thickness x is displayed in Fig. 11 for trilayers grown on GaAs(001) as well as on MgO(001). For both cases, there is no sharp maximum for the total coupling strength $J=J_1+J_2$ but an almost constant value of $|J|$ of the order of 1 mJ/m^2. This value is well comparable to those typically found for fully metallic systems[29] but is clearly smaller than the 6 mJ/m^2 observed for MBE-grown Fe/Si/Fe(001) trilayers.[30] We relate the reduced coupling strength compared to MBE samples to intermixing at the Fe/Si interface due to the higher energy of the incident particles during the sputtering process. In order to get an idea of the degree of intermixing, we perform XRR measurements of GaAs/Fe/Si bilayer systems. The reflectivity data in Fig. 12 can be fitted best when assuming an Fe-rich FeSi layer at the Fe/Si interface. The thickness of the intermixed region is about 8 Å, i.e., of the order of the Si spacer thickness. Hence, the coupling is not mediated by a Si-rich or even pure Si interlayer but by a possibly metallic FeSi layer consistent with previous studies of sputtered Fe/Si systems[31,32] and spectroscopic measurements of sputtered Fe/Si multilayers by Carlisle *et al.*[33] A metallic spacer could be the reason for the increase in (bilinear) coupling strength at a Si thickness of 19 Å in Fig. 11(a), which possibly indicates oscillatory behavior of the coupling.

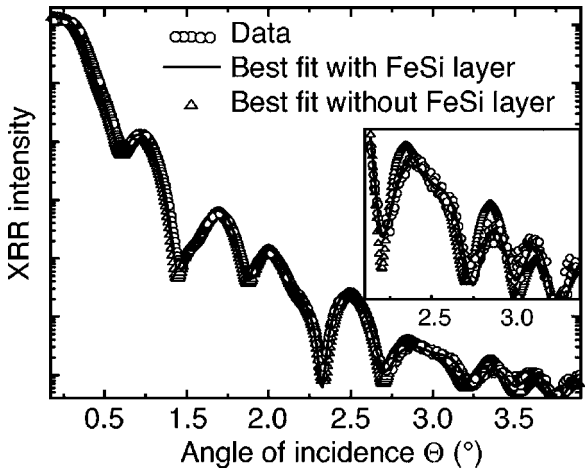

FIG. 12. XRR measurement of a GaAs/100 Å Fe/70 Å Si bilayer system deposited at 40 °C. Open circles represent data points, the solid line is the best fit including an FeSi layer, and triangles show the inferior fit for a sharp interface. The inset shows the magnified high-angle region of the diffractogram.

The hypothesis that enhanced intermixing reduces the coupling strength is confirmed in a further experiment, in which we increase the Si deposition rate by a factor of 2 from 0.3 to 0.6 Å/s in order to reduce diffusion and intermixing. Ion-beam sputtering allows us to keep all other sputtering parameters constant. As expected, the antiferromagnetic coupling strength increases. The maximum of the total coupling strength $|J|\approx 2$ mJ/m^2 at a Si thickness of 15 Å is larger by a factor of 2 and exceeds the coupling strengths previously reported for sputtered Fe/Si/Fe *trilayers*.[31,34,35] On the other hand, the coupling strength is similar to those found in sputtered, epitaxial, or polycrystalline Fe/Si *multilayers*.[31,32,36–38] Further experiments have to be performed to decrease the intermixing. One possibility is to vary the target angle φ, because the high-energetic Ar ions reflected towards the substrate are likely to intensify interdiffusion processes. Alternatively one could use a lower beam voltage to decrease the energy of the reflected particles.

IV. CONCLUSION

We have studied the growth of Fe single layers and Fe/Si/Fe trilayer systems on GaAs(001) and MgO(001) by ion-beam sputtering. Monocrystalline and epitaxial growth is achieved on both substrate types. The magnetic properties of Fe films on MgO substrates are superior to those of Fe films on GaAs. Surprisingly, monocrystalline and epitaxial growth of Fe films with a good quality is also possible on untreated, oxidized GaAs substrates. Our experiments—in particular, the absence of the interface-induced uniaxial anisotropy—clearly show that the oxide layer remains between GaAs and Fe. In this context one could think of spin injection experiments from Fe into GaAs through the native oxide layer, similar to van't Erve *et al.*,[39] who demonstrated a high spin injection efficiency in a GaAs/Al_2O_3/Fe system. Using an optimized set of sputtering parameters that lead to the best results for the growth of Fe on GaAs, Fe/Si/Fe(001) trilayer systems are grown and show strong antiferromagnetic interlayer exchange coupling. These results represent a further indication of the high crystalline growth quality achievable by ion-beam sputtering. For the best trilayers we measure a total coupling strength of 2 mJ/m^2.

[1]S. Datta and B. Das, Appl. Phys. Lett. **56**, 665 (1990).
[2]S. A. Wolf, D. D. Awschalom, R. A. Buhrman, J. M. Daughton, S. von Molnár, M. L. Roukes, A. Y. Chtchelkanova, and D. M. Treger, Science **294**, 1488 (2001).
[3]H. J. Zhu, M. Ramsteiner, H. Kostial, M. Wassermeier, H.-P. Schönherr, and K. H. Ploog, Phys. Rev. Lett. **87**, 016601 (2001).
[4]J. J. Krebs, B. T. Jonker, and G. A. Prinz, J. Appl. Phys. **61**, 2596 (1987).
[5]R. W. Tustison, T. Varitimos, J. van Hook, and E. F. Schloemann, Appl. Phys. Lett. **51**, 285 (1987).
[6]S. D. Bernstein, T. Y. Wong, and R. W. Tustison, J. Vac. Sci. Technol. A **17**, 571 (1999).
[7]S. D. Bernstein, T. Y. Wong, and R. W. Tustison, J. Vac. Sci. Technol. B **12**, 605 (1994).
[8]F. Monteverde, A. Michel, Ph. Guérin, and J.-P. Eymery, Surf. Sci. **482–485**, 872 (2001).
[9]F. Monteverde, A. Michel, J.-P. Eymery, and Ph. Guérin, J. Cryst. Growth **267**, 231 (2004).
[10]S. Kreuzer, K. Prügl, G. Bayreuther, and D. Weiss, Thin Solid Films **318**, 219 (1998).
[11]S. D. Bernstein, T. Y. Wong, and R. W. Tustison, J. Appl. Phys. **72**, 4358 (1992).
[12]D. E. Bürgler, C. M. Schmidt, J. A. Wolf, T. M. Schaub, and H.-J. Güntherodt, Surf. Sci. **366**, 295 (1996).
[13]M. Zölfl, M. Brockmann, M. Köhler, S. Kreuzer, T. Schweinböck, S. Miethaner, F. Bensch, and G. Bayreuther, J. Magn. Magn. Mater. **175**, 16 (1997).
[14]M. Gester, C. Daboo, R. J. Hicken, S. J. Gray, A. Ercole, and J. A. C. Bland, J. Appl. Phys. **80**, 347 (1996).
[15]R. Moosbühler, F. Bensch, M. Dumm, and G. Bayreuther, J. Appl. Phys. **91**, 8757 (2002).
[16]M. Brockmann, M. Zölfl, S. Miethaner, and G. Bayreuther, J. Magn. Magn. Mater. **198–199**, 384 (1999).
[17]B. Heinrich and J. F. Cochran, Adv. Phys. **42**, 523 (1993).
[18]M. Farle, Rep. Prog. Phys. **61**, 755 (1998).
[19]B. D. Cullity, *Introduction to Magnetic Materials* (Addison-Wesley, Reading, MA, 1972).
[20]B. Degroote, M. Major, J. Meersschaut, J. Dekoster, and G. Langouche, Surf. Sci. **482–485**, 1090 (2001).
[21]B. B. Maranville, A. L. Shapiro, F. Hellman, D. M. Schaadt, and E. T. Yu, Appl. Phys. Lett. **81**, 517 (2002).
[22]M. Rickart, T. Mewes, S. O. Demokritov, B. Hillebrands, and M. Scheib, Phys. Rev. B **70**, 060408 (2004).
[23]B. Li, J. R. Fermin, A. Azevedo, F. M. de Aguiar, and S. M. Rezende, Appl. Phys. Lett. **72**, 2760 (1998).
[24]X. W. Zhou and H. N. G. Wadley, J. Appl. Phys. **90**, 3359 (2001).
[25]T. R. Lundquist, J. Vac. Sci. Technol. **15**, 684 (1978).
[26]B. Window, J. Vac. Sci. Technol. A **11**, 1522 (1993).
[27]S. Iwatsubo, T. Takahashi, and M. Naoe, Thin Solid Films **281–282**, 484 (1996).
[28]M. Buchmeier, B. K. Kuanr, R. R. Gareev, D. E. Bürgler, and P. Grünberg, Phys. Rev. B **67**, 184404 (2003).
[29]D. E. Bürgler, P. Grünberg, S. O. Demokritov, and M. T. Johnson, in *Handbook of Magnetic Materials*, edited by K. H. J. Buschow (Elsevier, Amsterdam, 2001), Vol. 13, pp. 1–85.
[30]R. R. Gareev, D. E. Bürgler, M. Buchmeier, R. Schreiber, and P. Grünberg, J. Magn. Magn. Mater. **240**, 237 (2002).
[31]A. Chaiken, R. P. Michel, and C. T. Wang, J. Appl. Phys. **79**, 4772 (1996).
[32]E. E. Fullerton, J. E. Mattson, S. R. Lee, C. H. Sowers, Y. Y. Huang, G. Felcher, S. D. Bader, and F. T. Parker, J. Magn. Magn. Mater. **117**, L301 (1992).
[33]J. A. Carlisle, A. Chaiken, R. P. Michel, L. J. Terminello, J. J. Jia, T. A. Callcott, and D. L. Ederer, Phys. Rev. B **53**, R8824 (1996).
[34]K. Inomata, K. Yusu, and Y. Saito, Phys. Rev. Lett. **74**, 1863 (1995).
[35]Y. Endo, O. Kitakami, and Y. Shimada, J. Appl. Phys. **85**, 5741 (1999).
[36]T. Luciński, M. Kopcewicz, A. Hütten, H. Brückl, S. Heitmann, T. Hempel, and G. Reiss, J. Appl. Phys. **93**, 6501 (2003).
[37]J. Kohlhepp and F. J. A. den Broeder, J. Magn. Magn. Mater. **156**, 261 (1996).
[38]Y. Endo, O. Kitakami, and Y. Shimada, Phys. Rev. B **59**, 4279 (1999).
[39]O. M. J. van't Erve, G. Kioseoglou, A. T. Hanbicki, C. H. Li, B. T. Jonker, R. Mallory, M. Yasar, and A. Petrou, Appl. Phys. Lett. **84**, 4334 (2004).